A dimensional analysis of front-end bending in plate rolling applications

Denis Anders[1,2], Tobias Münker[3], Jens Artel[3], Kerstin Weinberg[2]

Abstract

Rolling under asymmetrical conditions such as temperature gradients within the material, difference of the circumferential velocity of the rolls and different friction coefficients cause the rolled slab to bend towards the direction of one of the rolls. This mechanical phenomenon is referred to as ski effect. In general this effect is undesired, since it hinders the further material transport and is a potential danger for the machine components in the proceeding processes. De facto it is possible to exert control on the ski effect in terms of selected peripheral speeds of the rolls. Unfortunately the essential mechanisms and the sensitivity of the influencing parameters in asymmetric rolling are still not comprehended sufficiently.

In this contribution a mathematical description of the ski effect is provided, embedding this process into a finite element framework of plasticity in the context of large deformations. In order to qualify the impact of specific process parameters a corresponding dimensional analysis is performed. The introduced dimensionless quantities give rise to a complete parametric study of the process under consideration. Both the ratio of the circumferential velocity of the rolls and the difference of the friction coefficients as a cause for ski effect are exposed and their influence as well as their interdependency subjected to different roll geometries are studied.

Key words: ski effect, asymmetric plate rolling, dimensional analysis, FE analysis

1. Introduction

Rolling mills represent an essential compound in industrial forming processes of slabs and sheets. During this forming process the work material is moved by rotating rolls continuously through an adjusted roll gap to undergo plastic deformations. The entire rolling procedure is extremely complex, because it is influenced by various system parameters such as temperature, initial thickness of the rolled stock, circumferential velocity of the rolls, the friction between the rolled stock and the rolls, the geometry of the roll gap, etc.

Under realistic manufacturing conditions, the forming process in rolling mills is subjected to asymmetric

[1]Corresponding author (Denis Anders),telephone /-fax: +49-271-740-2225 /-4644.
[2]Chair of Solid Mechanics, University of Siegen, Paul-Bonatz-Straße 9-11, 57068 Siegen, Germany
[3]Department of research and development, SMS Siemag AG, Wiesenstraße 30, 57271 Hilchenbach, Germany
Email addresses: Tobias.Muenker@SMS-Siemag.com (Tobias Münker), anders@imr.mb.uni-siegen.de (Tobias Münker), Jens.Artel@SMS-Siemag.com (Jens Artel), weinberg@imr.mb.uni-siegen.de (Kerstin Weinberg)

boundary conditions at the rolls due to a slight circumferential speed mismatch and different friction coefficients of the work rolls. This asymmetry leads to a turn-up (ski-up) or a turn-down (ski-down) of the front-end of the sheet leaving the roll gap. This phenomenon is usually referred to as so-called ski effect. An uncontrolled front-end bending in plate rolling applications may lead to losses in product quality and severe damage of the system components with expensive downtimes. Examples of several damage scenarios induced by uncontrolled front-end bending of the sheet (ski effect) are illustrated in Fig. 1.
Therefore, understanding the interplay of the essential system parameters and their influence on the ski effect is a great matter of interest to rolling mill engineers. The main objective is to choose the system variables in such a way that the bending curvature is kept very small. In some cases it is advantageous to adjust the plate bending slightly upwards in order to avoid overloading of the roll table.

(a) damage by turn-up (b) damage by turn-down

Figure 1: (a) illustrates a damage of the upper system components induced by upward bending of the rolled sheet. (b) shows a jammed sheet due to uncontrolled downward front-end bending.

Actually it is not the first time that the ski effect in asymmetric plate rolling is considered. Pan and Sansome (1982) derived a uniaxial analytical model to explore the characteristics of asymmetrical sheet rolling and compared it to experimental data thirty years ago. Jeswiet and Greene (1998) employed two-dimensional finite element simulations in order to quantify front-end bending in dependence of the roll surface speed. Kazeminezhad and Karimi Taheri (2005) added experimental investigations of the deformation behavior of carbon steel wires, studied the effect of processing variables like the friction coefficient and the rolling speed and derived some coarse guidelines to reduce the spreading of the wires after flat rolling. Analytical approaches to capture the rolling asymmetries by means of the slab method have been used by Hwang and Tzou (1993) to quantify rolling pressure, forces and torques and again by Hwang and Tzou (1995) taking effects of the shear stresses into account. However, both models do not consider curved sheets. The slab

method was therefore extended by Salimia and Sassani (2002) to predict the curvature of the rolled strip. Although analytical models based on slab methods provide a fast insight into the basic mechanisms of asymmetrical sheet rolling, they are inappropriate for a qualitative description of the ski effect. For this reason Pawelski (2000) studied friction effects in cold rolling by analyzing measured process data and some finite element simulations. Harrer et al. (2003) consider finite element analysis as an instrument to characterize asymmetric effects in plate rolling, in particular, the length-to-thickness shape factor and the speed mismatch. A detailed finite element based elastic-plastic analysis of the stress and strain distributions in the slab subjected to asymmetric rolling conditions is performed by Richelsen (1997). More emphasis on an advanced numerical method put Farhat-Nia et al. (2006) studying the development of the front-end curvature by means of two-dimensional (arbitrary Lagrangian-Eulerian) finite element simulations. A novel insight in the scope of measurement and control techniques on front-end bending phenomena is given by Kiefer and Kugi (2008a). They developed a semi-analytical approach utilizing the upper bound theorem in order to extract an efficient mathematical model for online execution in process control.

However, in this contribution extensive parametric studies of different front-end bending scenarios will be provided within a consistent elasto-plastic finite element framework. In this context it will be demonstrated how different rolling conditions affect the bending curvature.

Hence this manuscript is organized as follows. Motivated by the pioneer work of Pawelski (1992) who was one of the first researchers bringing metal forming aspects into the framework of the theory of similarity, in Section 2 a novel approach to characterize the front-end bending effect by means of dimensionless system variables is presented. Since the set of the employed dimensionless variables is formally derived in the context of the Vashy-Buckingham Π-theorem, a concise introduction into the basic concepts of dimensional analysis is given. Section 3 is devoted to detailed parametric studies within a consistent two-dimensional finite element framework. In conclusion, the obtained simulation results are outlined and critically discussed.

2. Dimansional analysis

The systematic analysis of complex physical settings by means of computational methods is extremely elaborate, because in real systems various physical quantities interact or compete simultaneously to finally determine the configuration of the system. To keep the computational cost at a reasonable level on the one hand and to provide a sufficient mathematical approximation to the problem under consideration on the other hand, it is important to specify the dominant physical quantities and to limit the parameter space of interest.

A very elegant technique to systematically reduce the number of influencing variables is the concept of dimensional analysis. The idea behind dimensional analysis is rather simple but also very effective. Here, one makes use of the fact that every physical equation has to satisfy the requirement of dimensional homogeneity.

This means that all the terms of a physical equation must have the same dimensions. The Vashy-Buckingham Π-theorem, which was first introduced by Vashy (1892) but is more connected to the famous work of Buckingham (1914), embeds dimensional analysis into an algebraic consideration. Let the considered system be determined by n physical quantities $Q_1, Q_2, \ldots, Q_n$ and let k be the number of arbitrary units needed as a basis to express the dimension/unit of $[Q_1], [Q_2], \ldots, [Q_n]$. Then the Π-theorem states that any physical relation

$$\Phi\left(Q_1, Q_2, \ldots, Q_n\right) = 0, \tag{1}$$

with physical quantities $Q_j \neq 0$, is equivalent to a relation of the form

$$\Psi\left(\Pi_1, \Pi_2, \ldots, \Pi_{n-k}\right) = 0. \tag{2}$$

In Eq. (2) the quantities $\Pi_1, \Pi_2, \ldots, \Pi_{n-k}$ denote dimensionless combinations given by

$$\Pi_i = \prod_{j=1}^{n} Q_j^{a_{ij}} \quad \text{for } i = 1, \ldots, n-k, \tag{3}$$

where the coefficient matrix

$$\mathbf{A} := \begin{pmatrix} a_{11} & \cdots & a_{1n} \\ \vdots & \ddots & \vdots \\ a_{(n-k)1} & \cdots & a_{(n-k)n} \end{pmatrix} \tag{4}$$

has rank $n - k$. Please note that the new relation (2) involves k fewer variables than the original relation (1).

Throughout this contribution SI-units will be employed as fundamental basis for unit representation, details are summarized in the National Institute of Standards and Technology publication of Taylor and Thomson (2008). The SI-unit convention gives a system of seven base units each representing different kinds of physical quantities, cf. tab. 1. In the most general consideration involving all physical quantities from tab. 1 there are $k = 7$ base units. For the dimensional analysis of front-end bending the SI base units for length [L], mass [M] and time [T] are considered.

In the next step it is important to figure out the crucial factors which influence front-end bending. In the present framework the set of influencing quantities is subdivided into two classes. The first class contains all parameters which lead to asymmetric conditions in the plate rolling process inducing the ski effect such as mismatch in circumferential speed, difference in radius of the rolls and unequal coefficients of friction. This class of system parameters is denoted as primary factors. The second class consists of parameters which do not induce front-end bending but they affect the amount of curvature when the ski effect is fully developed. Such parameters are pass reduction, slab thickness and the level of the friction coefficients.

base quantity (symbol)	dimension symbol	unit	name
length (l, x, r, etc.)	L	m	meter
mass (m)	M	kg	kilogram
time (t)	T	s	second
electric current (I, i)	I	A	ampere
thermodynamic temperature (T)	Θ	K	kelvin
luminous intensity (I_v)	J	cd	candela
amount of substance (n)	N	mol	mole

Table 1: SI base units and their corresponding physical quantities.

Tab. 2 outlines the influencing physical and geometrical quantities considered in the present model of front-end bending. Fig. 2 illustrates these quantities within the roll gap.

influencing variable	symbol	typical range
circumferential velocity (upper roll)	v_t	$0-3\frac{\mathrm{m}}{\mathrm{s}}$ (theor. value)
circumferential velocity (bottom roll)	v_b	$0-3\frac{\mathrm{m}}{\mathrm{s}}$ (theor. value)
radius (upper roll)	r_t	$400\,\mathrm{mm}-800\,\mathrm{mm}$
radius (bottom roll)	r_b	$400\,\mathrm{mm}-800\,\mathrm{mm}$
coefficient of friction (upper roll)	μ_t	$0.3-0.5$
coefficient of friction (bottom roll)	μ_b	$0.3-0.5$
plate entry thickness	h_0	$30\,\mathrm{mm}-200\,\mathrm{mm}$
plate exit thickness	h_1	$10\,\mathrm{mm}-180\,\mathrm{mm}$
yield point	k_f	$50\frac{\mathrm{N}}{\mathrm{mm}^2}-300\frac{\mathrm{N}}{\mathrm{mm}^2}$

Table 2: Influencing variables and their typical values in rolling processes.

A very comprehensive survey of alternative strategies to apply ideas from the theory of similarity on problems from forming technology was elaborated on by Pawelski (1993). Please note that in this contribution temperature induced front-end bending phenomena due to asymmetrical vertical temperature gradients in the slab are not considered. A detailed scientific treatise on this topic using a semi-analytical approach was

given by Kiefer and Kugi (2008b). They detected that vertical temperature gradients in the slab make the material always bending towards the cooler part of the rolled plate.

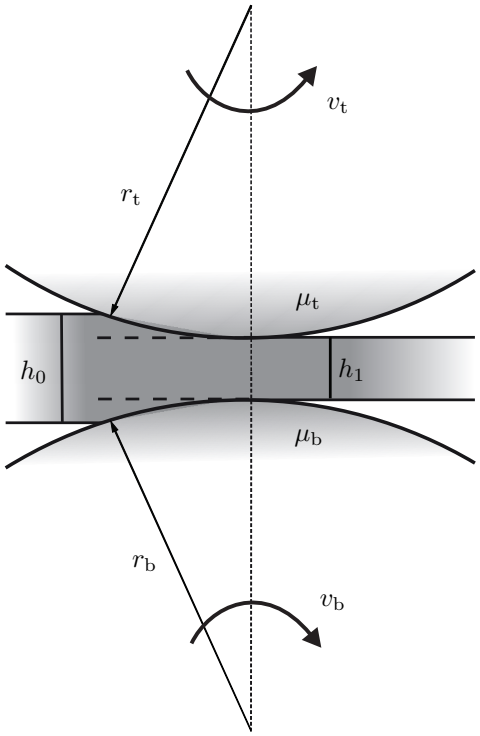

Figure 2: Illustration of geometric quantities within the roll gap.

2.1. Dimensional analysis of slab curvature

By means of the Vashy-Buckingham Π-theorem it is possible to derive a minimal set of dimensionless combinations to capture the front-end curvature. Since the mismatch of radii of rolls in modern plate mills is negligible it is admissible to set $R = r_\mathrm{t} = r_\mathrm{b}$. The coefficients of friction μ_t and μ_b are already dimensionless. Therefore, these system parameters will be regarded as dimensionless Π-quantities Π_4 and Π_5, respectively. The other dimensionless combinations are derived according to Eq. (3) by

$$\Pi_i = k_f^{a_{i1}} v_\mathrm{t}^{a_{i2}} v_\mathrm{b}^{a_{i3}} h_0^{a_{i4}} h_1^{a_{i5}} R^{a_{i6}} \kappa^{a_{i7}}. \tag{5}$$

Keeping in mind that the coefficient matrix $\mathbf{A} = (a_{ij}) \in \mathbb{R}^{7\times 4}$ must have rank$= n - k = 7 - 3 = 4$, one consequently obtains the following dimensionless combinations

$$\begin{aligned} \Pi_1 &= \frac{h_1}{h_0}, \qquad \Pi_2 = \frac{h_0}{R}, \qquad \Pi_3 = \frac{v_\mathrm{t}}{v_\mathrm{b}}, \\ \Pi_4 &= \mu_\mathrm{t}, \qquad \Pi_5 = \mu_\mathrm{b}, \qquad \Pi_6 = \kappa R \end{aligned} \tag{6}$$

with the corresponding coefficient matrix

$$\mathbf{A} = \begin{pmatrix} 0 & 0 & 0 & -1 & 1 & 0 & 0 \\ 0 & 0 & 0 & 1 & 0 & -1 & 0 \\ 0 & 1 & -1 & 0 & 0 & 0 & 0 \\ 0 & 0 & 0 & 0 & 0 & 1 & 1 \end{pmatrix}. \tag{7}$$

For the construction of dimensionless Π-numbers it is appropriate to combine similar physical quantities such as length type terms, velocity type terms, etc. However, Π_1 and Π_2 contain all relevant geometric quantities of the roll gap. In many technical applications the relative pass reduction

$$\varepsilon_h = 1 - \frac{h_1}{h_0} = 1 - \Pi_1 \tag{8}$$

is often used to measure the geometry of the roll gap. For a constant R the quantity Π_2 is proportional to the height of the rolled stock. The Π-number Π_3 indicates the speed mismatch. The dimensionless combination $\Pi_6 \in [-1, 1]$ measures the curvature of the plate where it is -1 or 1 if and only if the rolled slab has the same curvature as the bottom or the upper roll, respectively.

2.2. Dimensionless combinations for technological quantities

Likewise the calculations in Section 2.1 it is possible to derive dimensionless combinations for technological quantities such as the rolling torque of the upper/bottom roll $M_\mathrm{t}/M_\mathrm{b}$ and the rolling force F. These physical quantities can actually be measured during the forming process. For this reason, they are denoted as technological quantities.

Please note that here the dimensionless combinations $\Pi_1, \Pi_2, \ldots, \Pi_6$ are retained from the previous considerations. Analogously to the previous section the additional dimensionless combinations involving force and torque type terms are given by

$$\Pi_7 = \frac{M_\mathrm{t}}{k_f R^3}, \quad \Pi_8 = \frac{M_\mathrm{b}}{k_f R^3}, \quad \Pi_9 = \frac{F}{k_f R^2}. \tag{9}$$

The radius of the upper and bottom roll acts here as a geometrical reference value. In this manner the calculated Π-values are always related to the geometry of the rolls which take the forces and torques from the forming process.

The established dimensionless combinations from this section will serve as basis for the parametric studies in the sections below.

3. Finite element simulation

This section deals with a systematic finite element approach to the phenomenon of front-end bending by means of the dimensionless combinations from the previous part of the manuscript. Although numerous

investigations on front-end bending in plate rolling applications have been published in the past, according to Philipp et al. (2007) operators are still struggling with the problem. Therefore, detailed parametric studies will be provided here. These studies may be employed as reference for online implementation of control mechanisms during the forming process.

3.1. Finite element model

In the scope of this work the numerical simulations are performed by means of the commercial finite element software MSC.Marc/Mentat. Within the framework of this finite element model the work rolls are regarded as ideally rigid bodies rotating with the constant circumferential velocities v_t and v_b, respectively. The distance between the rolls is h_1. The roll table is modeled as a straight line which uniformly directs the slab into the roll gap and inhibits the movement of the slab in vertical direction. The friction between roll table and slab is neglected. The slab has the height h_0 and is modeled as a deformable body. Consequently, isoparametric quadrilateral elements with linear shape functions for the spatial discretization of the slab are employed. The velocity v_s of the slab is initially set to the mean velocity of v_t and v_b. Later on, the velocity of the slab is controlled by the angular velocities of the rolls so that the initial velocity v_s which is necessary to initialize the contact of the slab with the rolls does not affect the result of the simulation. The numerical algorithm for the contact between the slab and the upper/bottom work roll involves the Coulomb law of friction by means of friction coefficients $\mu_\mathrm{t}/\mu_\mathrm{b}$. For the sake of simplicity three-dimensional deformation phenomena such as spreading of the processed material within the roll gap are neglected. Therefore, a plane strain state in the two-dimensional Euclidean space characterized by spatial coordinates $\mathbf{x} := x_1\mathbf{e}_1 + x_2\mathbf{e}_2 = (x_1, x_2)$ may be assumed. Here, the basis vector $\mathbf{e}_1$ points into the horizontal rolling direction and $\mathbf{e}_2$ denotes the vertical direction referring to the height of the rolled sheet. Let $\mathbf{v} = \partial\mathbf{x}/\partial t \in \mathbb{R}^2$ be the spatial velocity field and $\boldsymbol{\sigma} \in \mathbb{R}^{3\times3}$ denotes the Cauchy stress tensor. In classical metal forming calculations external body forces like gravitational forces are neglected and the processed material is assumed to be incompressible. In terms of continuum mechanics these requirements are expressed for the quasi-static regime by means of the mass balance and the balance of linear momentum as follows

$$\mathrm{div}\,(\mathbf{v}) = 0, \tag{10}$$

$$\mathrm{div}\,(\boldsymbol{\sigma}) = \mathbf{0}. \tag{11}$$

As constitutive equation for the considered plastic deformation the classical von Mises flow rule

$$f = \left\| \frac{1}{2}\left(\boldsymbol{\sigma} - \frac{1}{3}\mathrm{tr}\,(\boldsymbol{\sigma})\right)\right\| - k_f \tag{12}$$

is used. After the yield stress k_f is reached the deformation of material is assumed to behave ideally rigid-plastic. Strain hardening as well as viscoplasticity are not considered in this model. Therefore, the system of

partial differential equations (10)-(12) subjected to given boundary conditions has to be solved. Please note that high computational costs as mentioned in Kiefer and Kugi (2008b) could be reduced with a coarser mesh in the areas which do not undergo a deformation in the roll gap. A very similar finite element model is used by Kiefer and Kugi (2008b) for the validation of their upper bound approach and by Richelsen (1997) to analyze the stress/strain distribution within the roll gap.

The result of one simulation is shown in Fig. 3. One can see the bending of the plate towards the upper roll and the asymmetric distribution of the slab's velocities over the roll gap.

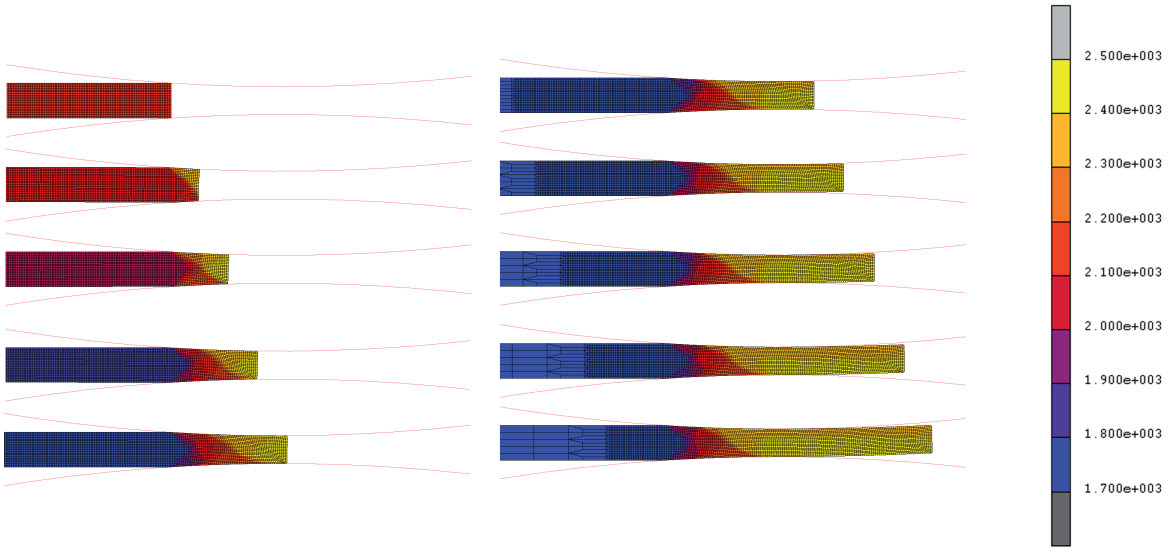

Figure 3: Illustration of finite element simulation results for the asymmetric rolling process with local velocities [mm/s].

In order to find a measure of the curvature of the slab a discrete curvature model is derived. After a sufficient time the state in the roll gap can be regarded as stationary. Hence, the slab's curvature κ is as well constant in time and front-end leaving the roll gap bends along a circle contour. Since the deformed configuration of the slab is here addressed by finite elements, the local curvature of the slab can be approximated with a circle through three nodes of the finite element mesh. This is schematically demonstrated in Fig. 4. For the center of the distances between theses nodes it holds

$$x_{m1} = \frac{x_1 + x_2}{2}, \qquad y_{m1} = \frac{y_1 + y_2}{2}, \tag{13}$$

$$x_{m2} = \frac{x_2 + x_3}{2}, \qquad y_{m2} = \frac{y_2 + y_3}{2}. \tag{14}$$

Let the linear equations of the perpendicular bisectors be:

$$m_1(x) = a_1 x + b_1 \tag{15}$$

$$m_2(x) = a_2 x + b_2 \tag{16}$$

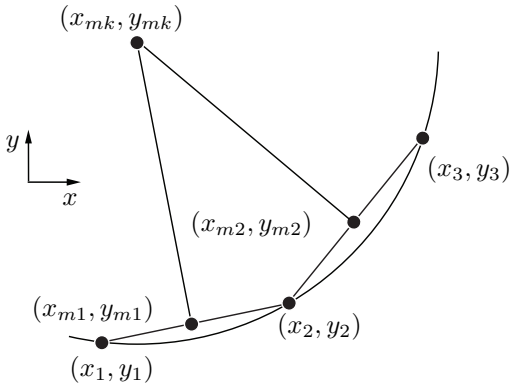

Figure 4: Schematic derivation of a discrete measure for curvature.

For the slopes and the axis intercepts one obtain:

$$a_1 = \frac{x_1 - x_2}{y_2 - y_1} \qquad b_1 = y_{m1} - a_1 x_{m1} \tag{17}$$

$$a_2 = \frac{x_2 - x_3}{y_3 - y_2} \qquad b_2 = y_{m2} - a_2 x_{m2} \tag{18}$$

The center of the circle (x_{mk}, y_{mk}) is the intersection point of the perpendicular bisectors.

$$a_1 x_{mk} + b_1 = a_2 x_{mk} + b_2 \tag{19}$$

$$\Leftrightarrow \quad x_{mk} = \frac{b_2 - b_1}{a_1 - a_2} \tag{20}$$

For y_{mk} it ensues

$$y_{mk} = m_1(x_{mk}). \tag{21}$$

The radius of the circle directly follows from the distance of the center point to an arbitrary construction point. Since the curvature of the slab is the reciprocal of the circle's radius, κ can be calculated according to

$$\kappa = \frac{1}{\sqrt{(y_{mk} - y_2)^2 + (x_{mk} - x_2)^2}} \tag{22}$$

3.2. Parametric studies

In the sequel, detailed parametric studies will be performed in order to get a deeper insight into front-end bending in plate rolling applications. Starting from the above-mentioned finite element model the following studies are embedded into a discrete parameter space spanned by the dimensionless combinations $\Pi_1, \Pi_2, \Pi_3, \Pi_4$ and Π_5. Whilst taking into account the technically relevant range for geometric quantities, speed mismatch and coefficients of friction between the upper and lower work roll and the material,

respectively, leads to the following parametric grid

$$\begin{aligned}
\Pi_1 &= [0.70, \quad 0.75, \quad 0.80, \quad 0.85, \quad 0.90, \quad 0.95] \\
\Pi_2 &= [0.02, \quad 0.04, \quad 0.06, \quad 0.08, \quad 0.10] \\
\Pi_3 &= [1.00, \quad 1.01, \quad 1.025, \quad 1.05] \\
\Pi_4 &= [0.30, \quad 0.40, \quad 0.50] \\
\Pi_5 &= [0.30, \quad 0.40, \quad 0.50]
\end{aligned} \tag{23}$$

Please note that for equal circumferential velocities $v_\mathrm{t} = v_\mathrm{b}$ ($\Pi_3 = 1$) and equal coefficients of frictions $\mu_\mathrm{t} = \mu_\mathrm{b}$ ($\Pi_4 = \Pi_5$) the forming process is fully symmetric and there is actually no front-end bending.
The mathematical quantification of the ski effect is done in terms of the dimensionless combination Π_6 which is proportional to the curvature κ. In the presented framework, a negative value of Π_6 indicates that the slab bends towards the bottom work roll.

3.2.1. Impact of friction conditions

Here the effect of the level of friction coefficients on the slab curvature at a fixed speed mismatch of 5% is studied. The simulation results are presented in two dimensional countour plots on $\Pi_1 \times \Pi_2$ illustrating respective isolines. In the first setting symmetric friction conditions subjected to the above-mentioned speed mismatch are considered. The results are shown in Figs. 5 – 7.

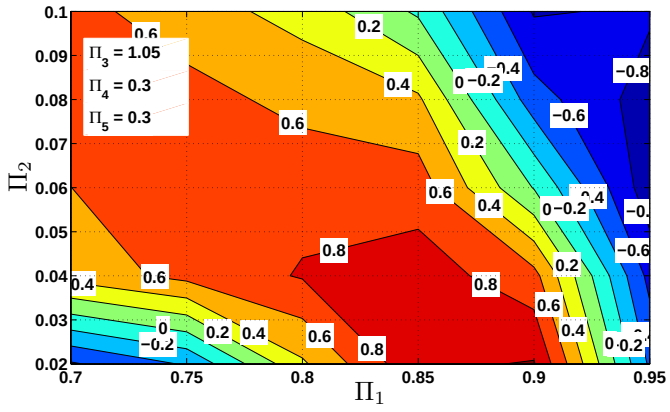

Figure 5: Illustration of Π_6 for $\Pi_4 = \Pi_5 = 0.3$ for a speed mismatch of 5%.

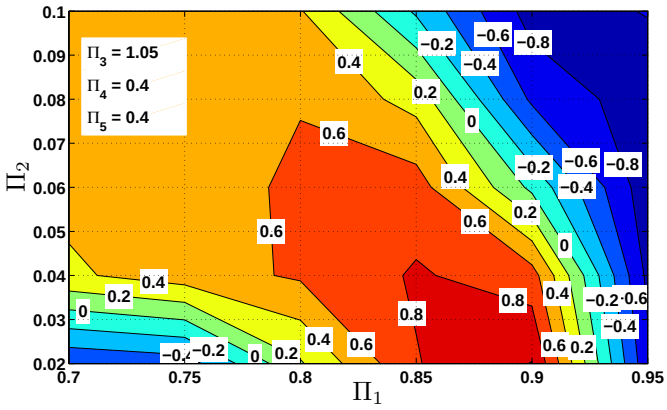

Figure 6: Illustration of Π_6 for $\Pi_4 = \Pi_5 = 0.4$ for a speed mismatch of 5%.

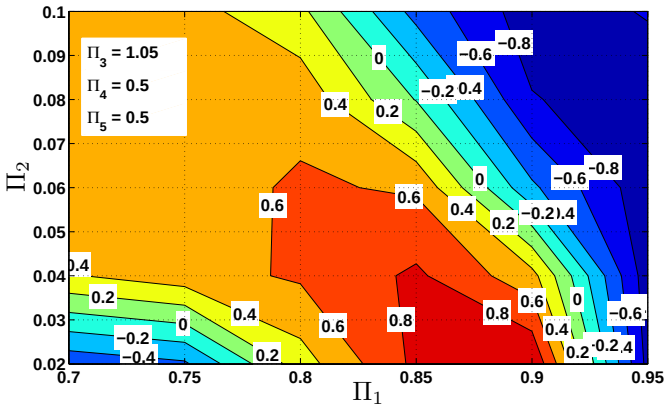

Figure 7: Illustration of Π_6 for $\Pi_4 = \Pi_5 = 0.5$ for a speed mismatch of 5%.

These results nicely reproduce the interesting fact that the curvature of the outgoing plate does not only depend on the asymmetric rolling conditions but also on the roll gap geometry, which has also been observed by Philipp et al. (2007) and Kiefer and Kugi (2008a). So far, it generally had been assumed that for plate rolling applications subjected to a speed mismatch of the work rolls the slab bends away from the faster roll for small thickness reductions and towards the faster roll for larger thickness reductions. This is actually the case for $(\Pi_1, \Pi_2) \in [0.80, 0.95] \times [0.04, 0.10]$. Surprisingly, the presented studies detect a further purely geometrical parameter setting with $(\Pi_1, \Pi_2) \in [0.7, 0.75] \times [0.02, 0.03]$ where the curvature is negative again. This result indicates that front-end bending is an extremely complex and highly nonlinear phenomenon, which is rather difficult to handle at the first glance.

The differences between Figs. 5 – 7 are very small, because the isoline where there is a change of sign of the curvature marginally varies. Therefore, one may state that the level of friction coefficients has a minor influence on the ski effect.

In the next setting asymmetric friction conditions at different levels associated with a speed mismatch of 5% are considered. The simulation results are illustrated in Figs. 8 – 13.

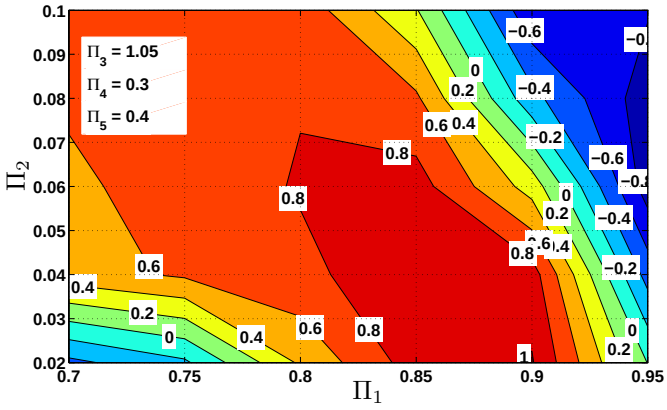

Figure 8: Illustration of Π_6 for asymmetric friction coefficients $\mu_t = 0.3$, $\mu_b = 0.4$ subjected to a speed mismatch of 5%.

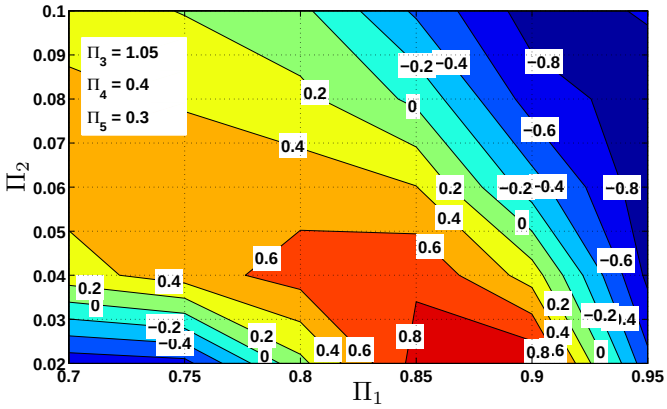

Figure 9: Illustration of Π_6 for asymmetric friction coefficients $\mu_t = 0.4$, $\mu_b = 0.3$ subjected to a speed mismatch of 5%.

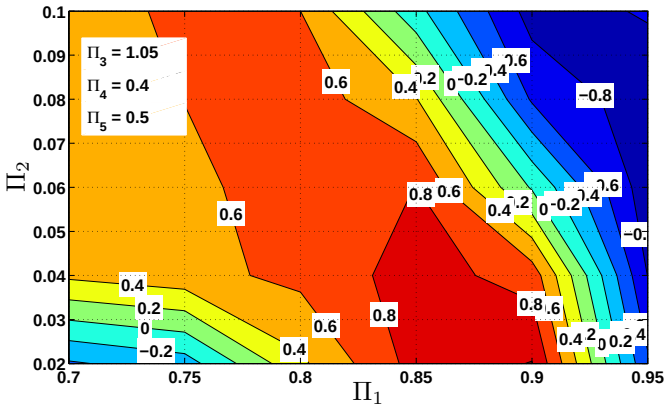

Figure 10: Illustration of Π_6 for asymmetric friction coefficients $\mu_t = 0.4$, $\mu_b = 0.5$ subjected to a speed mismatch of 5%.

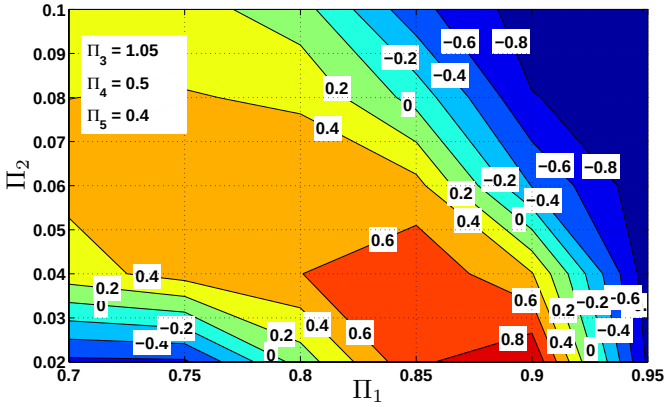

Figure 11: Illustration of Π_6 for asymmetric friction coefficients $\mu_t = 0.5$, $\mu_b = 0.4$ subjected to a speed mismatch of 5%.

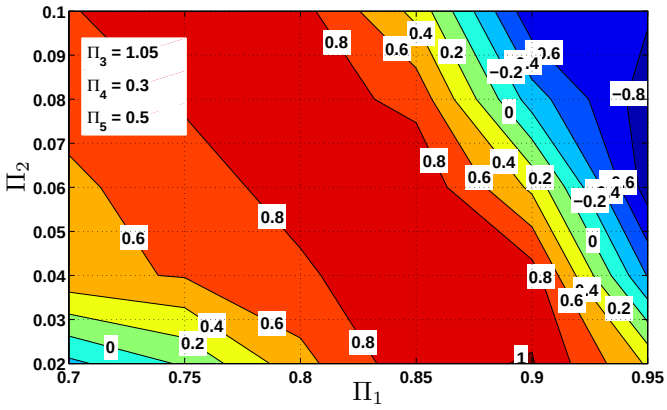

Figure 12: Illustration of Π_6 for asymmetric friction coefficients $\mu_t = 0.3$, $\mu_b = 0.5$ subjected to a speed mismatch of 5%.

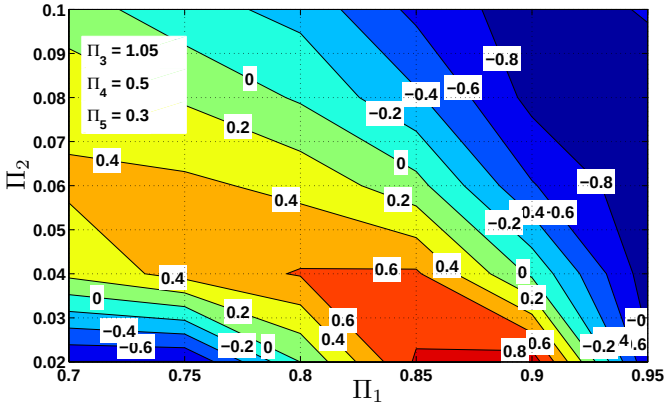

Figure 13: Illustration of Π_6 for asymmetric friction coefficients $\mu_t = 0.5$, $\mu_b = 0.3$ subjected to a speed mismatch of 5%.

In all figures one observes that the 5% speed mismatch has a much stronger impact on the ski effect compared to asymmetric friction conditions. Here, the order of magnitude of the front-end curvature is affected slightly in the asymmetric friction regime in comparision with the setting in Figs. 5 – 7. Even a 40% asymmetry in friction coefficients is insufficient to compensate a 5% speed mismatch. Therefore technically relevant variations of friction coefficients cannot convert the ski effect due to a 5% speed mismatch. Nevertheless, the influence of asymmetric friction coefficients is apparent. The obtained results indicate that asymmetric friction conditions encourage a front-end bending towards the work roll with the lower coefficient of friction.

Switching off the speed mismatch by setting $\Pi_3 = 1$, one sees that the effect of asymmetric friction coefficients is independent of the roll gap geometry in contrast to the observations made for the influence of speed mismatch in Figs. 5 – 7. In Figs. 14 – 16 the independence of the roll gap geometry for pure friction asymmetry can be seen in the fact that Π_6 does not change sign in the parameter space $\Pi_1 \times \Pi_2$. As already mentioned in the previous setting, a pure friction asymmetry has quantitatively a smaller effect on front-end bending as speed mismatches. The order of magnitude of bending curvature in a setting with 25% friction asymmetry, see Figs. 14 and 15, is about 0.2 (in average of the absolute value) and about 0.35 in the 40% asymmetric friction setting, see Fig. 16.

More extensive studies on other parametric settings may be found in the appendix.

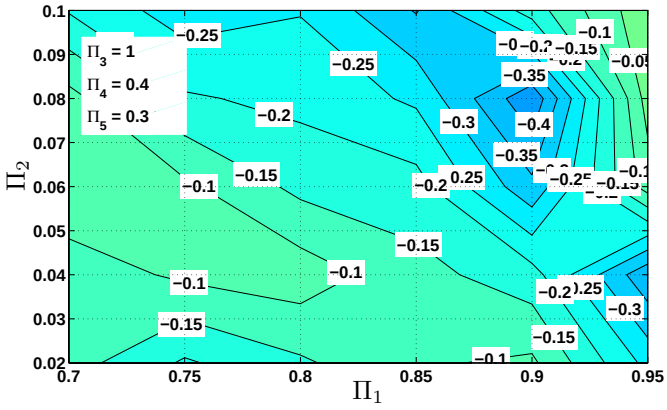

Figure 14: Illustration of Π_6 for asymmetric friction coefficients $\mu_t = 0.4$, $\mu_b = 0.3$ without a speed mismatch.

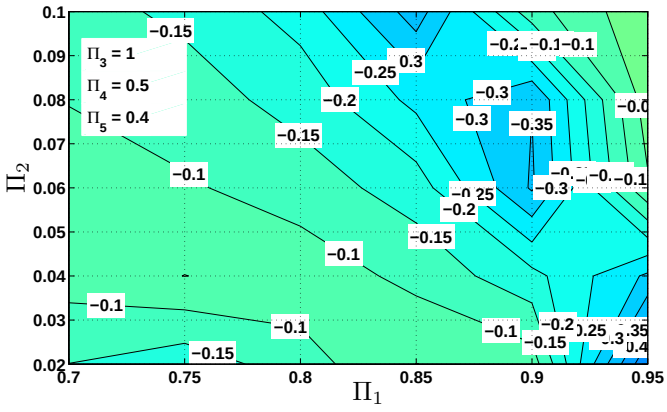

Figure 15: Illustration of Π_6 for asymmetric friction coefficients $\mu_t = 0.5$, $\mu_b = 0.4$ without a speed mismatch.

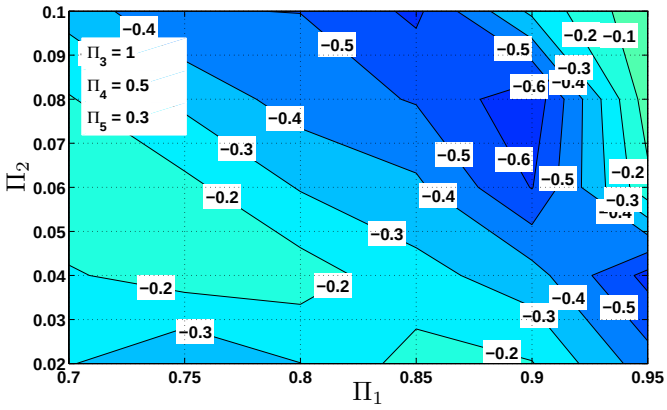

Figure 16: Illustration of Π_6 for asymmetric friction coefficients $\mu_\mathrm{t} = 0.5$, $\mu_\mathrm{b} = 0.3$ without a speed mismatch.

3.2.2. Reference to the shape factor

In most publications on metal forming the roll gap geometry is described by the so-called shape factor

$$s = \frac{l_d}{h_m} = \frac{\sqrt{R\,(h_0 - h_1)}}{\frac{h_0+h_1}{2}}, \tag{24}$$

which is defined as the ratio of the arc length of contact l_d and the medium thickness h_m of the plate. By means of relations

$$h_1 = \Pi_1 \cdot h_0 \quad \text{and} \quad R = \frac{h_0}{\Pi_2} \tag{25}$$

it is possible to express the shape factor (24) in terms of the dimensionless combinations Π_1 and Π_2 according to

$$s\,(\Pi_1, \Pi_2) = \frac{2\sqrt{\frac{1}{\Pi_2}\,(1 - \Pi_1)}}{1 + \Pi_1}. \tag{26}$$

Fig. 17 presents a plot of isolines for $s = 1.3$ and $s = 1.6$ embedded into the simulation results within the parameter space $\Pi_1 \times \Pi_2$. For $\Pi_2 > 0.03$ it turns out that the domain where the curvature of the slab changes its sign is fully enclosed by the isolines of the given shape factors. Unfortunately, the shape factor is insufficient to predict the change in curvature for great values of pass reduction accompanied by small values of Π_2. However, the shape factor is a suitable characteristic value for a first rough estimation of the ski effect. Please note that this estimation is only valid for $(\Pi_1, \Pi_2) \in [0.80, 0.95] \times [0.04, 0.10]$, because an underestimation of the ski effect by the user may lead in the worst case scenario to a severe damage of the equipment components as already shown in Fig. 1.

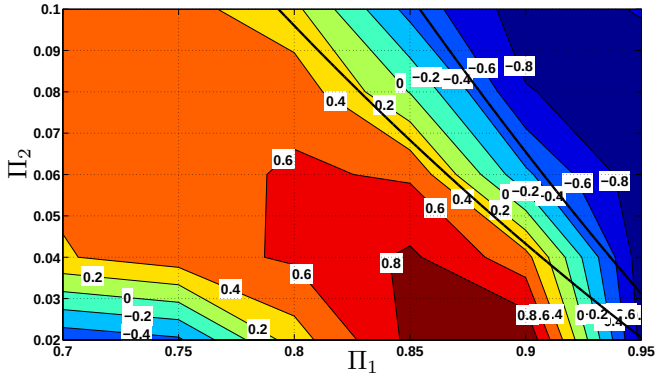

Figure 17: Illustration of the isolines for $s = 1.3$ and $s = 1.6$ with Π_6 for symmetric friction coefficients $\mu_t = \mu_b = 0.4$ subjected to a speed mismatch of 5%.

3.2.3. Qualitative analysis of the impact of friction

From the point of view of control engineers, it is worthwhile to check how a ski effect from inherent friction asymmetries may be compensated by a purposefully adjusted speed mismatch. To this end the qualitative effect of friction coefficients on the characteristic curvature Π_6 at a speed mismatch of 5% is illustrated in Figs. 18 and 19.

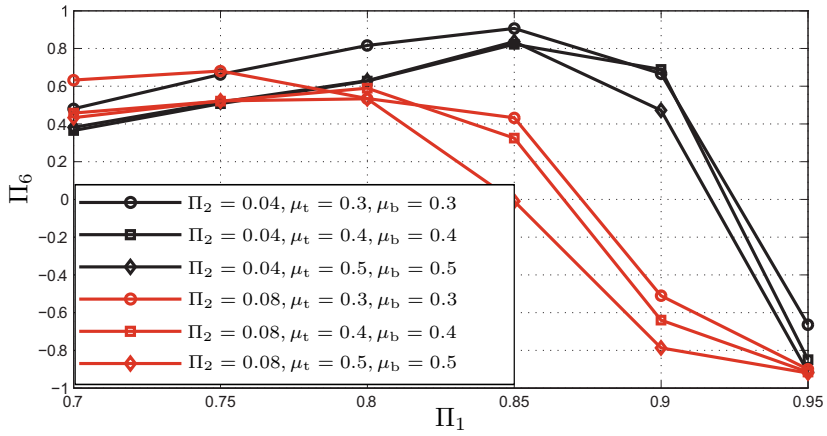

Figure 18: Change of characteristic curvature Π_6 subjected to a speed mismatch of 5% and variations of equal friction coefficients.

Fig. 18 indicates that the curves for $\Pi_2 = 0.04$ and $\Pi_2 = 0.08$ have a very similar shape in each case despite of local variations of about 0.4 at $\Pi_1 = 0.85$. Fig. 19 confirms the observation that the curvature of the coming out plate is not influenced by the absolute value of the friction coefficients. In fact, it is driven by the total amount of the difference between μ_t and μ_b.

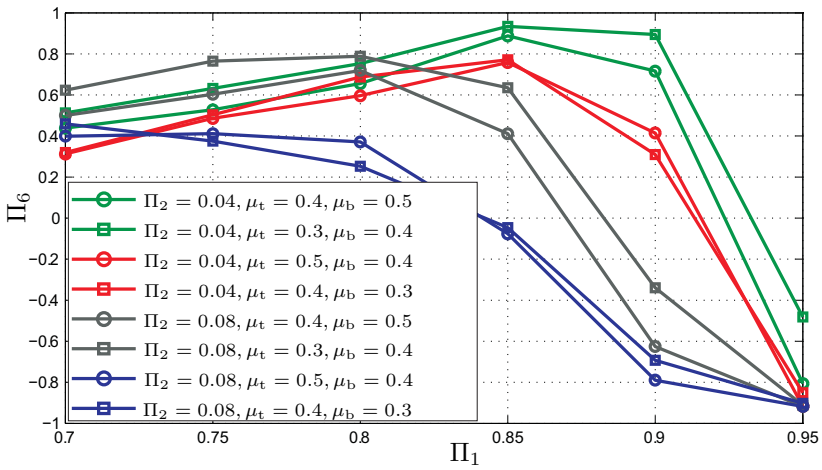

Figure 19: Change of characteristic curvature Π_6 subjected to a speed mismatch of 5% and variations of unequal friction coefficients.

3.2.4. Impact of different values for speed mismatch

So far, only speed mismatches of 5% are considered for the sake of clearness. Now it will be elaborated on the effect of different values of speed mismatch on the curvature of the front-end. The corresponding simulation results are outlined in Fig. 20. As a rule of thumb one can say that the formation of ski-ends increases with increasing speed mismatches. The domain where the front-end curvature changes its sign is approximately independent of the absolute value of the speed mismatch.

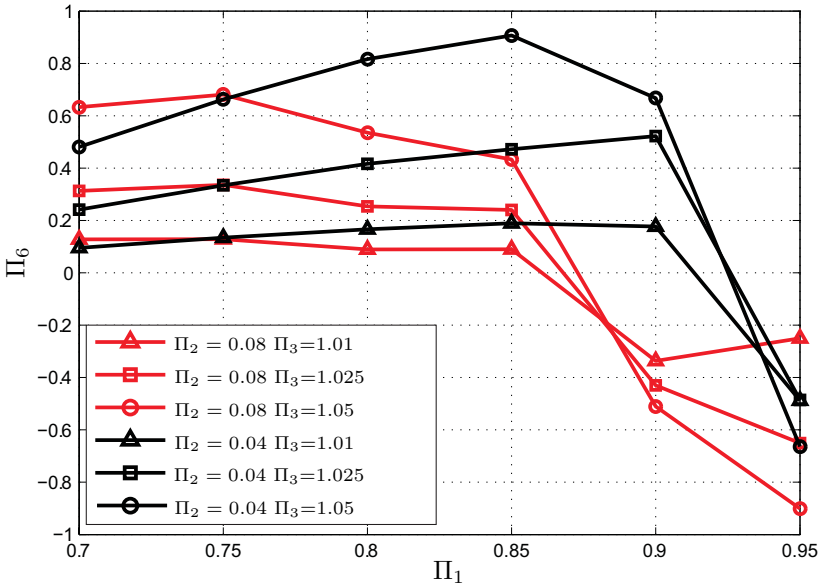

Figure 20: Influence of different values of speed mismatch on the characteristic curvature for $\mu_t = \mu_b = 0.3$.

3.2.5. Behavior of characteristic technological quantities

In this section a brief insight into the evolution of the dimensionless technological parameters Π_7, Π_8 and Π_9 during the forming process is given. During all simulations presented in Figs. 21 – 23 a speed mismatch of 5% and $\mu_t = \mu_b = 0.3$ is assumed. Fig. 21 clearly illustrates that the characteristic upper torque Π_7 (torque of the faster work roll) is always greater than the characteristic bottom torque Π_8 (torque of the slower work roll). In contrast to the torque of the upper work roll, the torque of the lower work roll strongly varies depending on the roll gap geometry, see Fig. 22. As one would expect, the rolling force increases with increasing pass reduction and slab thickness. This is nicely reproduced by the simulation results in Fig. 23.

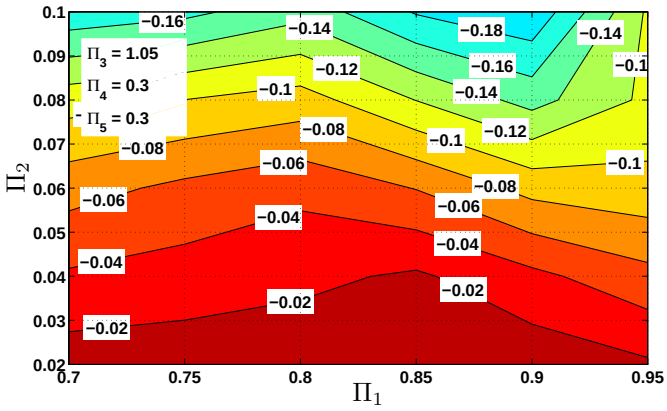

Figure 21: Illustration of the characteristic upper torque Π_7 for a speed mismatch of 5% and $\mu_t = \mu_b = 0.3$.

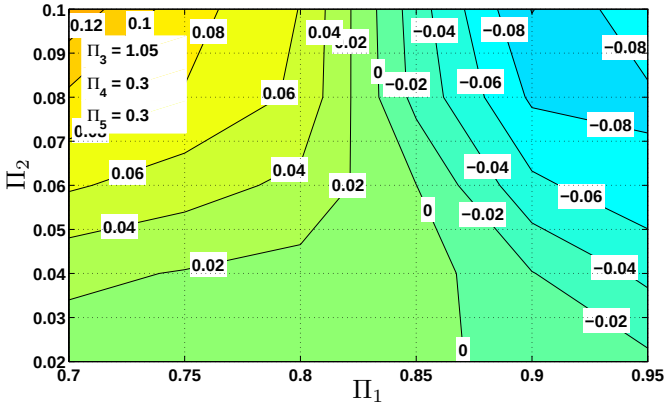

Figure 22: Illustration of the characteristic bottom torque Π_8 for a speed mismatch of 5% and $\mu_t = \mu_b = 0.3$.

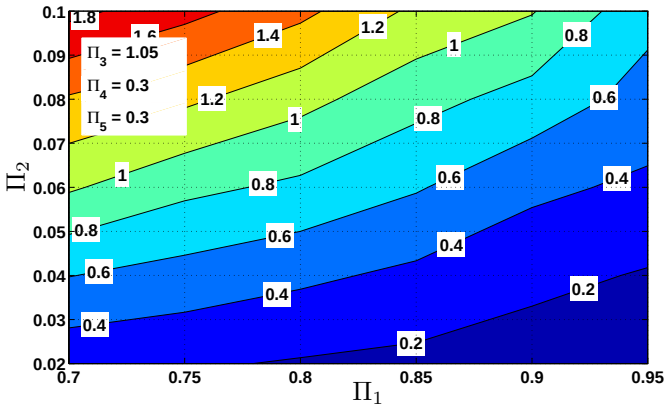

Figure 23: Illustration of the characteristic rolling force Π_9 for a speed mismatch of 5% and $\mu_t = \mu_b = 0.3$.

4. Conclusion

In this article, a novel approach for the description of front-end bending in asymmetrical rolling of plates is presented. For that purpose, this work accomplishes a dimensional analysis motivated by the concept of physical similarity in order to derive dimensionless groups which characterize the essential physics of the ski effect in rolling applications. The quality of the developed model was verified by means of systematic parametric studies in extensive finite element simulations. The investigations uncovered a new parameter setting in which the slab curvature changes its sign. So far, this phenomenon was not covered by frameworks associated to the shape factor as geometric reference value. In the setting of moderate pass reductions, where the application of the shape factor is a suitable representation of the roll gap geometry the novel approach reproduces as well the commonly known observation that the curvature of the outgoing plate changes sign for larger shape factors. Additionally, the presented simulation results strongly indicate that a speed mismatch during the rolling process has a greater effect on front-end bending than asymmetric friction conditions. Since front-end bending is a highly complex physical phenomenon it is not possible to provide an analytical explanation for this observation. In real technical applications, asymmetric friction conditions are always connected to slight speed mismatches of the work rolls and therefore they can hardly be regarded separately. This contribution provides a wide range of reference data for everyday use in rolling mills. In this context, the obtained results may serve as basis for the design and the implementation of control strategies to avoid or at least minimize the occurrence of ski-ends under asymmetrical rolling conditions.

References

Buckingham, E., 1914. On physically similar systems; Illustrations of the use of dimensional equations. Physical Review 4, 345–376.

Farhat-Nia, F., Salimi, M., Movahhedy, M.R., 2006. Elasto-plastic finite element simulation of asymmetrical plate rolling using an ALE approach. Journal of Materials Processing Technology 177, 525–529.

Hwang, Y.-M., Tzou, G.-Y., 1993. An analytical approach to asymmetrical cold strip rolling using the slab method. Journal of Engineering and Performance 2, 597–606.

Harrer, O., Philipp, M., Pokorny, I., 2003. Numerical simulation of asymmetric effects in plate rolling. Acta Metallurgica Slovaca 9, 306–313.

Hwang, Y.-M., Tzou, G.-Y., 1995. An analytical approach to asymmetrical hot-sheet rolling considering the effects of the shear stress and internal moment at the roll gap. Journal of Materials Processing Technology 52, 399–424.

Jeswiet, J., Greene, P.G., 1998. Experimental measurement of curl in rolling. Journal of Materials Processing Technology 84, 202–209.

Kazeminezhad, M., Karimi Taheri, A., 2005. An experimental investigation on the deformation behavior during wire flat rolling process. Journal of Materials Processing Technology 160, 313–320.

Kiefer, T., Kugi, A., 2008a. An analytical approach for modelling asymmetrical hot rolling of heavy plates. Mathematical and Computer Modelling of Dynamical Systems 14(3), 249–267.

Kiefer, T., Kugi, A., 2008b. Model-based control of front-end bending in hot rolling processes. Vortrag: 17th World Congress, The International Federation of Automatic Control, ; 06.07.2008 - 11.07.2008; In: "Proceedings of the 17th World Congress, The International Federation of Automatic Control, Seoul, Korea, July 6–11, ISSN: 1474–6670; pp. 1645–1650.

Pan, D., Sansome, D. H., 1982. An experimental study of the effect of roll-speed mismatch on the rolling load during the cold rolling of thin strip. Journal of Mechanical Working Technology 6, 361–377.

Pawelski, O., 1992. Ways and limits of the theory of similarity in application to problems of physics and metal forming. Journal of Materials Processing Technology 34(1–4), 19–30.

Pawelski, O., 1993. Ähnlichkeitstheorie in der Umformtechnik. In: Dahl, W., Kopp, R., Pawelski, O. (Eds.), Umformtechnik, Plastomechanik und Werkstoffkunde. Berlin, Springer, ISBN 3-50-56682-1, pp. 158–176

Pawelski, H., 2000. Comparison of methods for calculating the influence of asymmetry in strip and plate rolling. Steel research 71, 490–496.

Philipp, M., Schwenzfeier, W., Fischer, F.D., Wödlinger, R., Fischer, C., 2007. Front end bending in plate rolling influenced by circumferential speed mismatch and geometry. Journal of Materials Processing Technology 184(1–3), 224–232.

Richelsen, A. B., 1997. Elastic-plastic analysis of the stress and strain distributions in asymmetric rolling, International Journal of Mechanical Sciences 39(11), 1199–1211.

Salimia, M., Sassani, F., 2002. Modified slab analysis of asymmetrical plate rolling. International Journal of Mechanical Sciences 44, 1999–2023.

Taylor, B.N., Thompson, A., Editors, 2008. The International System of Units (SI). National Institute of Standards and Technology Special Publication 330.

Vaschy, A., 1892. Sur les lois de similitude en physique. Annales Télégraphiques (troisième série) 19, 25–28.

Appendix A. Diagrams of curvature coefficient Π_6 at different settings

This appendix will provide the reader with additional results on characteristic curvature Π_6 for various parameter settings.

Appendix A.1. Results for 2.5% speed mismatch

The first section focuses on front-end bending for a 2.5% speed mismatch subjected to different friction conditions. Throughout the simulation results it can be observed that for moderate values of the speed mismatch

asymmetries of friction coefficients have a much greater impact on the slab curvature, see Figs. A.24-A.32. Compared to the simulation results for the settings with a 5% speed mismatch, the parametric subdomain $\Omega \subset \Pi_1 \times \Pi_2$ associated with small curvature values $\Pi_6 \in [-0.2, 0.2]$ has a much greater overall fraction $\pi_\Omega := |\Omega| \,/\, |\Pi_1 \times \Pi_2|$ for smaller values of speed mismatch. For the 5% speed mismatch settings π_Ω roughly varies between 5-25%. In the 2.5% speed mismatch scenario the absolute values of fraction π_Ω are calculated about 5-50%. The maximum values for π_Ω are always achieved for $\mu_\mathrm{t} = 0.5$ and $\mu_\mathrm{b} = 0.3$ independent from the absolute value of speed mismatch $\Pi_3 > 1$. The smallest value for π_Ω is always obtained for $\mu_\mathrm{t} = 0.3$ and $\mu_\mathrm{b} = 0.5$. These results give a first hint that a superposition of effects from asymmetric friction conditions and an adequate speed mismatch may be used to equilibrate the forming process with respect to a minimal slab curvature.

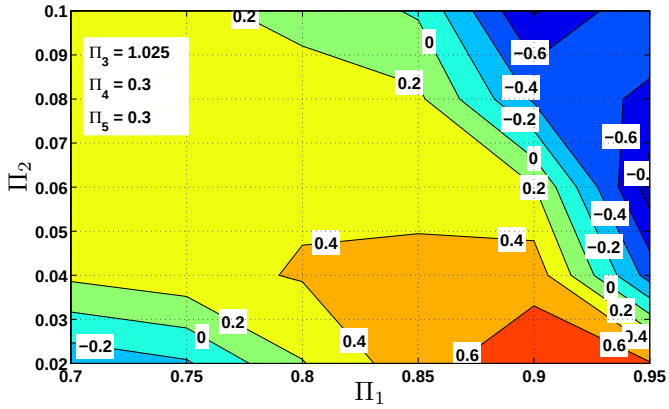

Figure A.24: Simulation results for $\Pi_3 = 1.025$, $\mu_\mathrm{t} = \mu_\mathrm{b} = 0.3$.

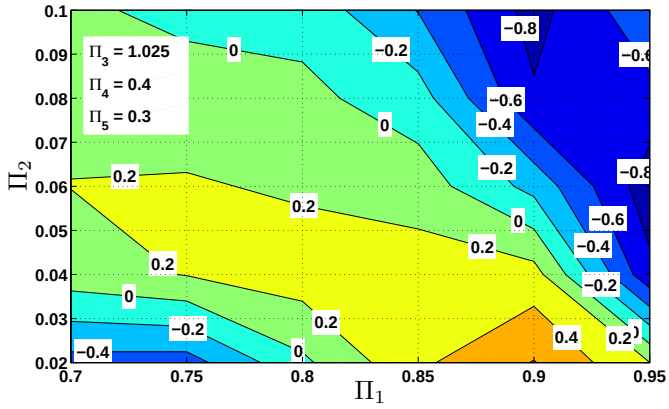

Figure A.25: Simulation results for $\Pi_3 = 1.025$, $\mu_\mathrm{t} = 0.4$ and $\mu_\mathrm{b} = 0.3$.

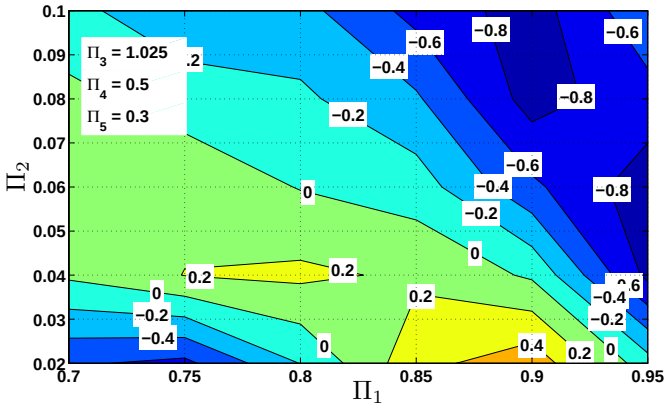

Figure A.26: Simulation results for $\Pi_3 = 1.025$, $\mu_\mathrm{t} = 0.5$ and $\mu_\mathrm{b} = 0.3$.

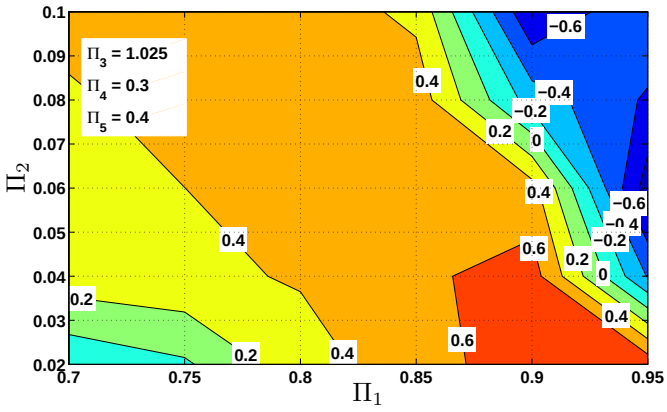

Figure A.27: Simulation results for $\Pi_3 = 1.025$, $\mu_\mathrm{t} = 0.3$ and $\mu_\mathrm{b} = 0.4$.

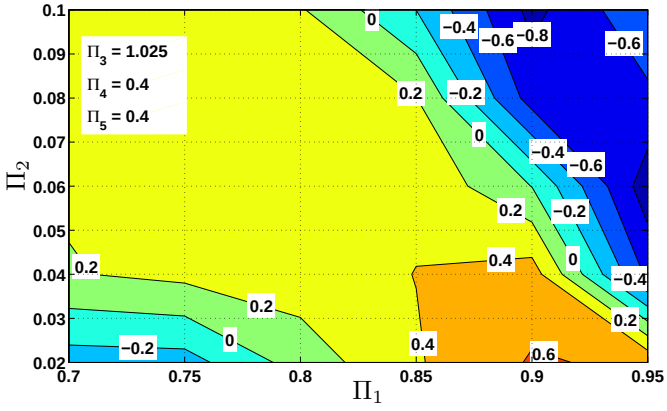

Figure A.28: Simulation results for $\Pi_3 = 1.025$, $\mu_\mathrm{t} = 0.4$ and $\mu_\mathrm{b} = 0.4$.

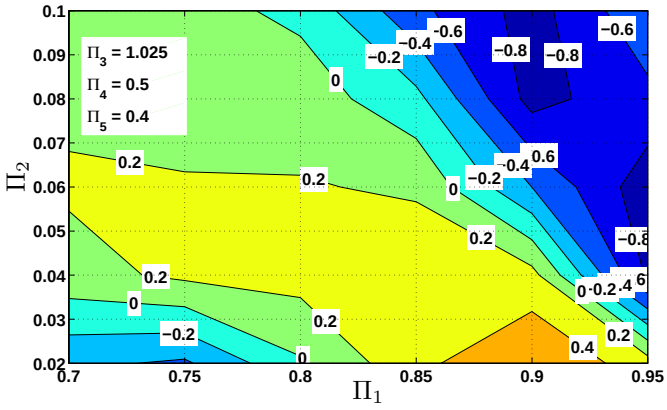

Figure A.29: Simulation results for $\Pi_3 = 1.025$, $\mu_t = 0.5$ and $\mu_b = 0.4$.

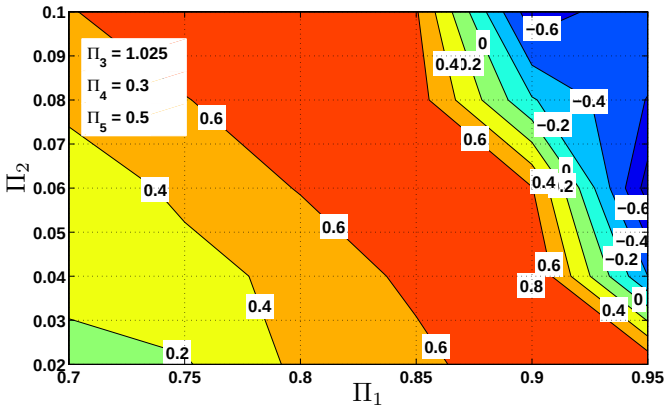

Figure A.30: Simulation results for $\Pi_3 = 1.025$, $\mu_t = 0.3$ and $\mu_b = 0.5$.

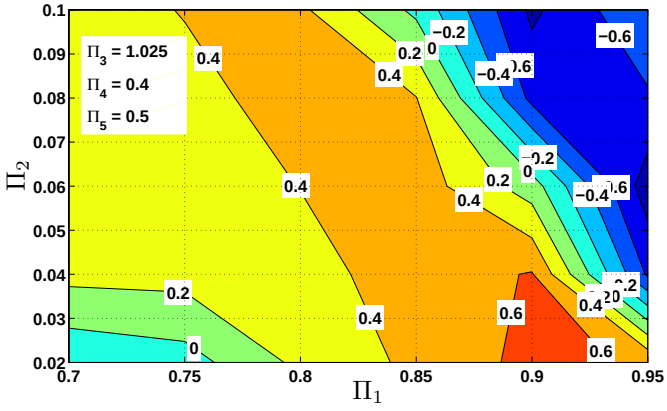

Figure A.31: Simulation results for $\Pi_3 = 1.025$, $\mu_t = 0.4$ and $\mu_b = 0.5$.

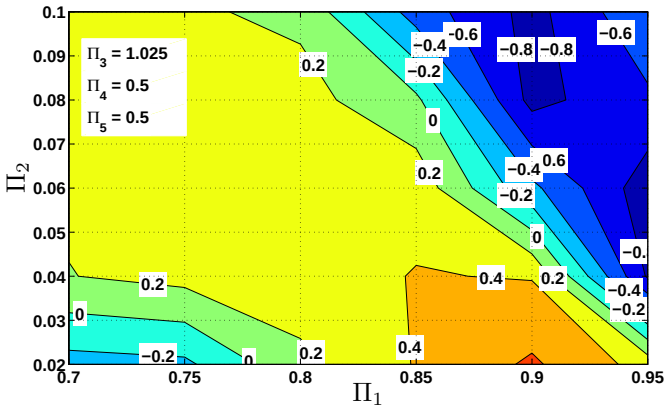

Figure A.32: Simulation results for $\Pi_3 = 1.025$, $\mu_\mathrm{t} = 0.5$ and $\mu_\mathrm{b} = 0.5$.

Appendix A.2. Results for 1% speed mismatch

In this section front-end bending events mainly driven by asymmetries in the friction conditions within the roll gap are considered. Here, the system is subjected to a rather slight speed mismatch of 1%. The obtained simulation results indicate that this speed mismatch may be employed to compensate certain asymmetric friction conditions, cf. Figs. A.33-A.41. In this context the values of π_Ω have an extremely broad range of 10-72.5%. Especially the setting with $\mu_\mathrm{t} = 0.5$ and $\mu_\mathrm{b} = 0.4$ where $\pi_\Omega \approx 72.5\%$ is of high interest, see Fig. A.38. In this very configuration the process is almost equilibrated for about 72.5% of the parameter space involving different geometries of the roll gap. This result corroborates the supposition from the previous section. It shows that ski effects due to asymmetric friction can be superimposed by slight speed mismatches to achieve an almost equilibrated rolling process with slight front-end bending.

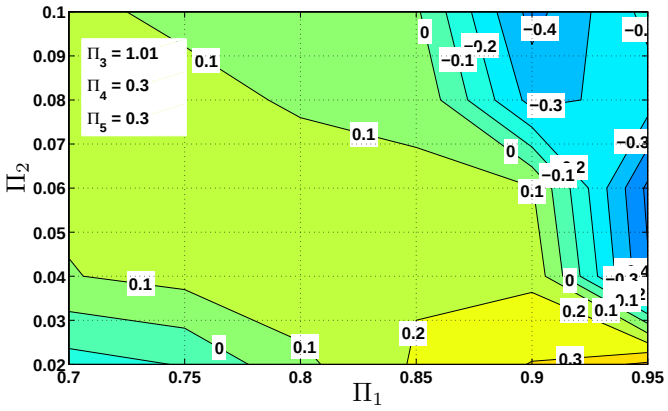

Figure A.33: Simulation results for $\Pi_3 = 1.01$, $\mu_\mathrm{t} = 0.3$ and $\mu_\mathrm{b} = 0.3$.

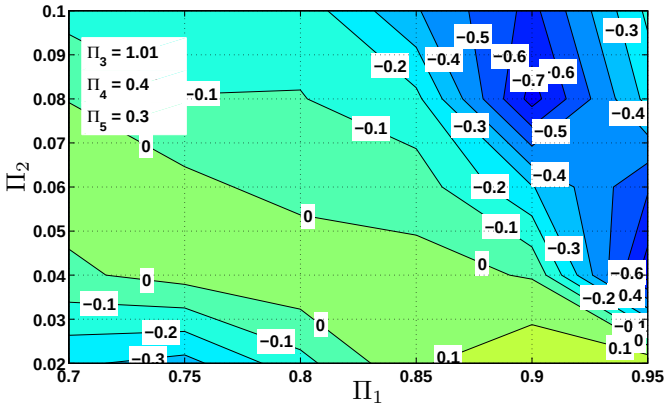

Figure A.34: Simulation results for $\Pi_3 = 1.01$, $\mu_t = 0.4$ and $\mu_b = 0.3$.

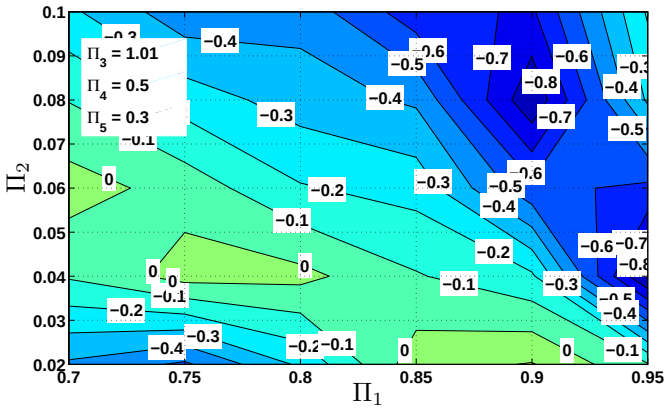

Figure A.35: Simulation results for $\Pi_3 = 1.01$, $\mu_t = 0.5$ and $\mu_b = 0.3$.

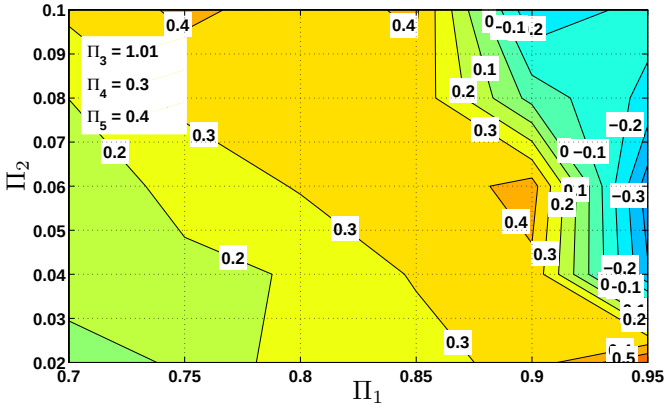

Figure A.36: Simulation results for $\Pi_3 = 1.01$, $\mu_t = 0.3$ and $\mu_b = 0.4$.

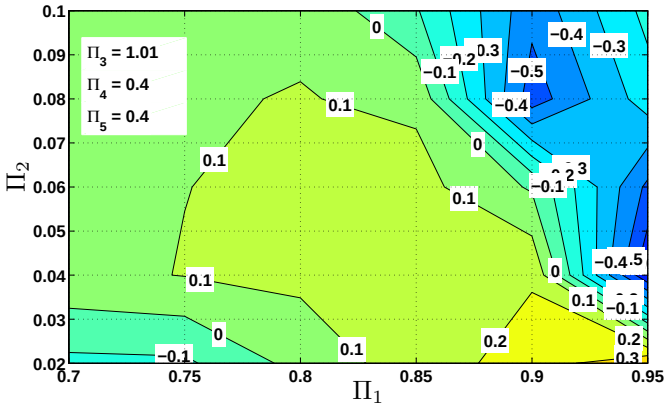

Figure A.37: Simulation results for $\Pi_3 = 1.01$, $\mu_t = 0.4$ and $\mu_b = 0.4$.

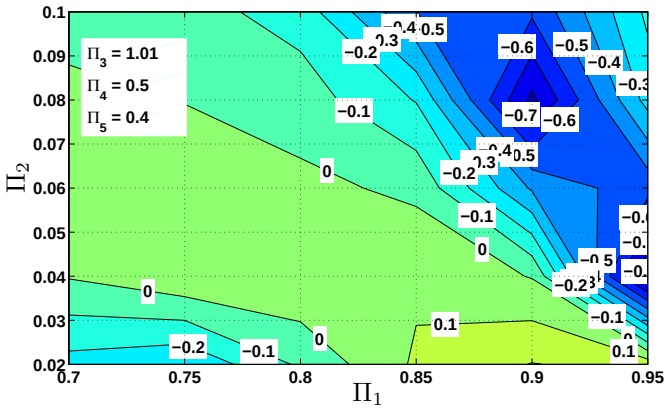

Figure A.38: Simulation results for $\Pi_3 = 1.01$, $\mu_t = 0.5$ and $\mu_b = 0.4$.

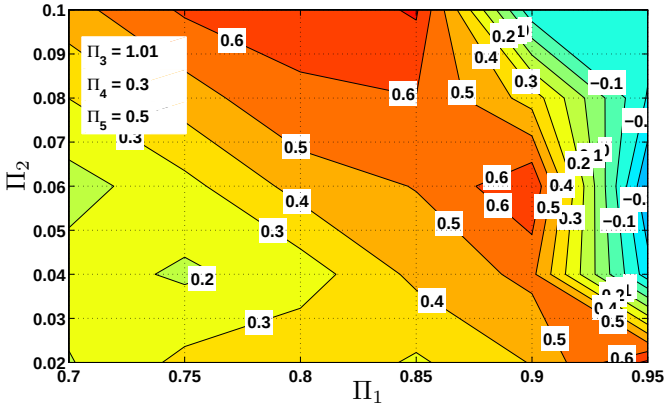

Figure A.39: Simulation results for $\Pi_3 = 1.01$, $\mu_t = 0.3$ and $\mu_b = 0.5$.

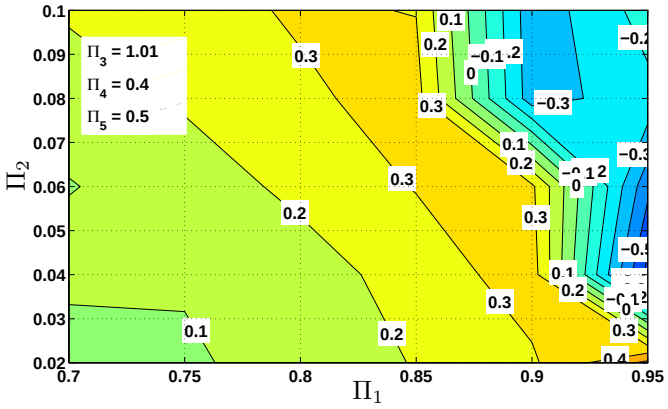

Figure A.40: Simulation results for $\Pi_3 = 1.01$, $\mu_t = 0.4$ and $\mu_b = 0.5$.

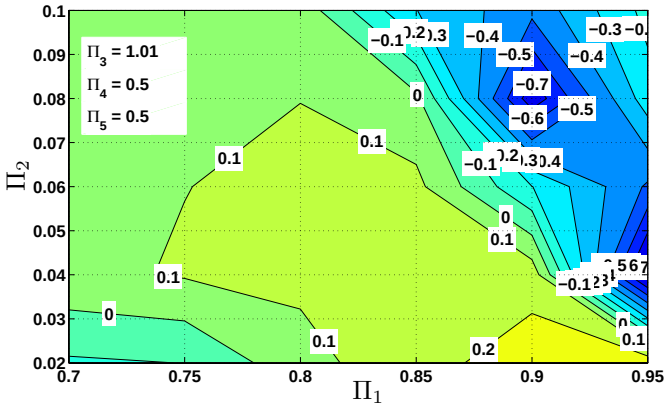

Figure A.41: Simulation results for $\Pi_3 = 1.01$, $\mu_t = 0.5$ and $\mu_b = 0.5$.